PERGAMON

International Journal of Heat and Mass Transfer 43 (2000) 921–933

International Journal of HEAT and MASS TRANSFER

www.elsevier.com/locate/ijhmt

Heat transfer analysis of a diffusion flame leading edge near a cold, chemically inert surface

Robert Vance*, Indrek S. Wichman

Department of Mechanical Engineering, Combustion Laboratory, Michigan State University, East Lansing, MI 48824-1226, USA

Received 25 November 1998; received in revised form 21 May 1999

Abstract

This numerical investigation of lifted diffusion flames examines the interaction of flame and surface from a heat transfer perspective. Conduction is the primary mode of heat loss from the laboratory-scale flame. Heat flux profiles to the lower chemically inert boundary are obtained for three different models: a finite-rate chemistry model, a simplified heat conduction model, and the limiting case Burke–Schumann model. Generalizations are made about the shape of the heat flux profiles to the anchoring boundary, as well as the practical usefulness of the presented models. A characteristic flame thickness is also defined from the generalized heat flux shape.

1. Introduction

Real flames interact with surfaces. These interactions may be primary, in which case the interaction of the flame with the surface cannot be ignored in an analysis of flame behavior, or secondary, in which case the solid surface is largely incidental to the combustion process. The flame-surface interaction includes many physical processes: flame chemistry; fluid flow dynamics; conductive, convective, and radiant heat transfer. For this reason a comprehensive theoretical model is exceedingly difficult, perhaps impossible, to construct. On the other hand, a pure numerical study without theoretical guidance is likely to make few novel observations. A similar statement applies of course to experimentation, thus suggesting that a 'democratic' investigation, in which every conceivable influence is equally weighted and seriously considered, will surely fail for not making distinctions between what is important and what is unimportant. Consequently, the development of theories for simplified limiting cases is a necessary part of a rational examination. Although theories almost by definition involve the suppression of some physics, this suppression ideally should have a positive, not a negative, aspect. This is adumbrated in the following quotation: "Idealization does not consist, as is commonly believed, in a subtracting or deducting of the petty and secondary. A tremendous expulsion of the principal features rather is the decisive thing, so that thereupon the others too disappear" [1]. Thus, it is the prominence of various model (theory) features which, by necessity, force the remaining features into the background. Finally, we note from practical experience that large-scale numerical simulations often employ simplistic 'sub-models' in order to describe processes that cannot be fully resolved by the global theory. It is imperative that such 'sub-models' faithfully represent the 'sub-problem' they purport to describe. They must

* Corresponding author.

E-mail addresses: vancerob@egr.msu.edu (R. Vance), wichman@egr.msu.edu (I.S. Wichman).

0017-9310/00/$ - see front matter
PII: S0017-9310(99)00193-3

Nomenclature

b	reduced Damkohler number
c_p	specific heat
D	binary diffusion coefficient
Da	Damkohler number
H	excess enthalpy
l	half channel width
N	non-dimensional spatial coordinate
Pe	Peclet number
q	heat flux
R	non-dimensional spatial coordinate
r_q	quenching distance, $(\xi^2+\eta^2)^{1/2}$ in ξ,η coordinates of Fig. 1
r_q'	quenching distance, $(u^2+v^2)^{1/2}$ in u, v coordinates of Fig. 2
S	scaling factor
T	temperature
u, v	dimensional conformal mapping coordinates
U, V	non-dimensional coordinates $(u/r_q, v/r_q)$
v	velocity
W	reaction term
w	non-dimensional reaction term
x, y	dimensional coordinates
Y_i	mass fraction of species i
y_i	non-dimensional mass fraction of species i
Z	mixture fraction
α	thermal diffusivity
α	$\alpha = 1 - T_0/T_f$
β	Zel'dovich number, $\beta = \alpha(E/RT_f)$
β_i	curve fit parameter
ϕ	global stoichiometric index
η	non-dimensional spatial coordinate
ϑ	heat transfer parameter detailed in (Eq. (22a))
λ	thermal conductivity
ν	ratio of oxidizer mass to fuel mass
θ	non-dimensional spatial coordinate
ρ	density
τ	non-dimensional temperature, $\tau = (T-T_0)/(T_f-T_0)$
Ξ, ξ	non-dimensional spatial coordinates
i	counter
F	fuel
f	flame
O	oxidizer
0	reference boundary value
q	quench

also be integrated with sufficient ease into the larger computation.

The purpose of this study is to first examine the leading edge of a flame in terms of the heat transfer during the quenching of a flame leading edge by an adjacent, cold, solid surface. The conductive heat transfer from a flame to a nearby surface is important for ensuring a continued supply of fuel, as in flame spread, or for ensuring flame survival, as in burner-attached flames. In the former case, the transfer of heat from the spreading flame gasifies the solid fuel beneath it, producing the fuel vapors that feed it with reactant. In the latter case, the heating of the burner rim by the flame minimizes transient heat losses, thereby maximizing reactant consumption while preventing possible flame extinction. Studies have recently been completed on various features of flame-wall interaction, in configurations reminiscent of both flame spread [2] and burner-attached flames [2,3].

A second feature of flame-surface interaction that we wish to investigate is the flame behavior as predicted by the relatively simple analysis of the conserved scalar mixture fraction combined with infinitely fast-rate chemical kinetics. As will be shown in comparisons to numerical solutions of the non-linear, finite-rate chemistry problem (model problem 'A'), the examination of the mixture fraction field can provide valuable insight into the flame quenching mechanism. In addition, the study of model problem 'A' provides the necessary impetus for examining the quenching problem discussed previously. Nevertheless, certain analytical solutions obtained by these means shall exhibit almost no correspondence with our detailed examination.

From a practical viewpoint, and in terms of material response, the most important quantity to examine is the conductive heat flux, both to the surface and at various locations in the gas. Radiative heat losses are ignored for two primary reasons: in small scale combustion, conductive losses are dominant [4] and under micro-gravity conditions, soot and gas radiation are generally diminished. Currently, we know very little about such conductive fluxes, including their characteristic orders of magnitude or their functional shapes. Although some progress has recently been made in this area [2], we are far from a satisfactory understanding that might enable the use of such estimates in any engineering capacity. Our analysis herein has features in common with Ref. [5], where the nature of the opposed-flow flame spread over solid fuels was examined in detail. The simplifications provided by employing infinite rate chemistry and an idealized geometry for gas flow and flame spread enabled numerous deductions to be made, which might otherwise have

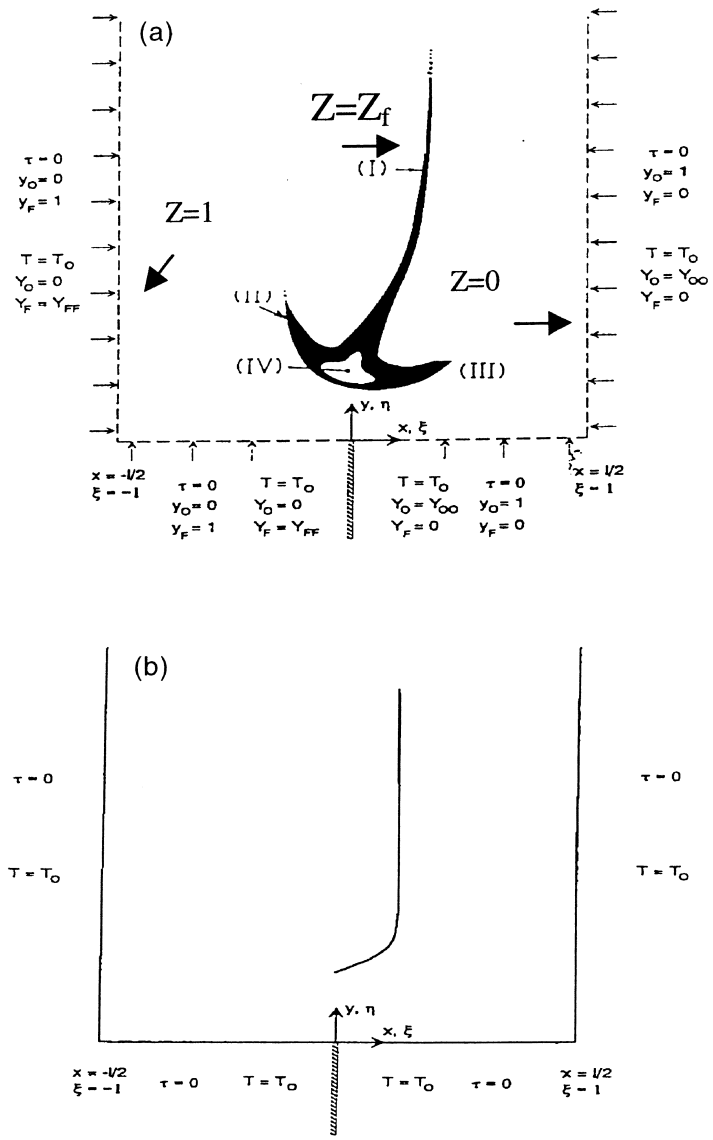

Fig. 1. (a) Model configuration and boundary conditions. The side and lower walls are porous to reactants. The vertical walls admit only diffusive fluxes. In the far field the diffusion flame is one-dimensional. The near field triple flame structure is shown, with (I) as the diffusion flame, (II) and (III) as rich and lean premixed flame arcs, and (IV) as the triple point or leading flame edge. (b) Heat transfer model for infinitesimally thin flame sheet and isothermal boundary conditions. This model is the heat transfer simplification of the flame in (a) because by far the greatest heat release is along the diffusion flame arc.

remained hidden in excessive detail. One of these was the seemingly paradoxical result, long since confirmed by numerical examination [6] that the streamwise conductivity through the solid fuel bed plays a minor, almost negligible, role in the rate of flame spread. In addition to the heat flux into walls and surfaces, it is also worth examining heat fluxes across various planes in the gas [5].

Of particular interest in our model problem is the flux directed from the flame leading edge towards the nearby surface. As discussed in Refs. [2,7], this flux can change significantly from very large values near the leading edge, where the flame quenches, to much smaller values near the surface, where the gas loses thermal energy to the wall.

2. Background

In this article, we shall examine a greatly simplified

heat transfer model problem (model 'B') in the light of a fuller (but still simplified) model 'A'. The latter includes finite-rate chemistry. It has been shown in past work that model 'A' is an often quantitatively accurate representation of the actual, physical problem [8]. This conclusion was reached by comparing flame behavior in model 'A' with a variable property Navier–Stokes simulation.

In this section, we shall restate and examine various previous results from the analysis of model 'A'. We shall also present various analytical results from this model for the infinite-rate chemistry limit. This examination will be conducted with the intent of providing motivation for a detailed examination of the pure heat transfer model 'B' in Sections 3–5.

Model 'A' describes qualitatively a fuel injector problem and more rudimentarily a general lifted triple flame resembling, but different in some features than, a flame-spread problem. The model configuration is shown in Fig. 1(a). The fuel flows past one side of an impermeable, perfectly conducting divider and mixes with the oxidizer stream that flows past its other side. Permeable walls through which fuel and oxidizer separately diffuse are aligned with the bulk flow direction, which is vertical. Depending on the global stoichiometry, the diffusion flame inclines either to the left, to the right, or lies directly downstream of the divider. This model produces a triple flame configuration with a premixed flame arc anchoring the diffusion flame to the lower boundary. The diffusion flame extends downstream from the anchor point. Fig. 1(a) shows a schematic of the triple flame configuration, including the fuel-rich and fuel-lean premixed flames and the trailing downstream diffusion flame arc. The system is assumed to be steady. All boundaries except the divider plate are porous, non-reactive walls, whose temperature is T_0. The velocities, v, of the two streams are identical and specified at the inlet boundary [9,10]. The chemical reaction between the fuel and oxidizer occurs through a single irreversible step. It has been shown [11,12] that, although not capturing all the quantitative characteristics of the flame, single step chemistry captures many qualitative characteristics such as flame structure and temperature. Furthermore, even in multi-step kinetics models, only a few reactions are responsible for a majority of the heat released during combustion. The molecular weights of the reactants are assumed identical, the thermophysical properties ρ, λ, c_p, D, are assumed constant, the Lewis numbers of the reactants are equal to unity, the influences are gravity and radiation (from the surface and the gas) are neglected, and Soret and Dufour terms are neglected. The diffusion velocities are given by Fick's law, and heat conduction is described by Fourier's law. Under these restrictions, the equations for conservation of species and energy become

$$\rho v\frac{\partial Y_0}{\partial y} = \rho D\nabla^2 Y_0 - \nu W \tag{1a}$$

$$\rho v\frac{\partial Y_F}{\partial y} = \rho D\nabla^2 Y_F - W \tag{1b}$$

$$\rho v c_p\frac{\partial T}{\partial y} = \rho\lambda\nabla^2 T + qW \tag{1c}$$

where $W = \rho A Y_O Y_F \exp(-E/RT)$ and the boundary conditions are

$$T = T_0, \quad Y_O = Y_{OO}, \quad Y_F = 0 \quad \text{at } (x = l/2, y \geq 0), (0 < x < l/2, y = 0) \tag{2a}$$

$$T = T_0, \quad Y_O = 0, \quad Y_F = Y_{FF} \quad \text{at } (x = -l/2, y \geq 0), (-l/2 < x < 0, y = 0) \tag{2b}$$

$$\frac{\partial T}{\partial y} = \frac{\partial Y_O}{\partial y} = \frac{\partial Y_F}{\partial y} = 0 \quad \text{at } y = \infty \tag{2c}$$

Eqs. (1a)–(1c) and (2a)–(2c) can be written more compactly in non-dimensional form. We rescale the independent variables with $l/2$ to obtain $\xi = x/(l/2)$, $\eta = y/(l/2)$ so that $\xi = \pm 1$ in the two corners of Fig. 1(a). The species mass fractions are normalized as $y_F = Y_F/Y_{FF}$, $y_O = Y_O/Y_{OO}$. Hence, both y_F and y_O are bounded by zero and unity. Similarly, the non-dimensional temperature is $\tau = (T - T_0)/(T_f - T_0)$, whereby $\tau = 0$ on all boundaries and $\tau \to 1$ at the flame sheet. Finally, the non-dimensional mass flux past the divider is $Pe = \rho v c_p L/\lambda$. Additional physical quantities, which are important to our subsequent analysis, are the global stoichiometric index

$$\varphi = \frac{\nu Y_{FF}}{Y_{OO}} \tag{3}$$

where ν is the ratio of mass of oxidizer to mass of fuel in the one-step reaction; the Zel'dovich number β, which is a measure of the temperature sensitivity of the reaction

$$\beta = \alpha\frac{E}{RT}, \quad \alpha = 1 - \frac{T_0}{T_f}; \tag{4}$$

the Damkohler number, Da, as a ratio of the diffusion time to the reaction time

$$Da = \frac{L^2/(\lambda/\rho c_p)}{\left[A Y_{OO}\exp(-E/RT_f)\right]^{-1}} \tag{5}$$

With the adiabatic flame temperature T_f defined as $T_f = T_0 + Q Y_{FF}/c_p(1+\phi)$, the non-dimensional reac-

tion term becomes

$$w = y_O y_F \exp\left[\frac{-\beta(1-\tau)}{1-\alpha(1-\tau)}\right] \tag{6}$$

The non-dimensional conservation Eqs. (1a)–(1c) can now be written as

$$Pe\frac{\partial y_O}{\partial \eta} = \nabla^2 y_O - \varphi Daw \tag{7a}$$

$$Pe\frac{\partial y_F}{\partial \eta} = \nabla^2 y_F - Daw \tag{7b}$$

$$Pe\frac{\partial \tau}{\partial \eta} = \nabla^2 \tau + (1+\varphi)Daw \tag{7c}$$

with $\nabla^2 = \partial^2/\partial\xi^2 + \partial^2/\partial\eta^2$. The dimensionless Eqs. (2a)–(2c) become

$$\tau = 0, \quad y_O = 0, \quad y_F = 1 \quad \text{at } (\xi = -1, \eta \geq 0), (-1 < \xi < 0, \eta = 0) \tag{8a}$$

$$\tau = 0, \quad y_O = 1, \quad y_F = 0 \quad \text{at } (\xi = 1, \eta \geq 0), (0 < \xi < 1, \eta = 0) \tag{8b}$$

$$\frac{\partial \tau}{\partial \eta} = \frac{\partial y_O}{\partial \eta} = \frac{\partial y_F}{\partial \eta} = 0 \quad \text{as } \eta \to \infty \tag{8c}$$

Eqs. (7a)–(7c) and (8a)–(8c) can be formulated in terms of the excess enthalpy function $H = \tau + y_O + y_F - 1$, the mixture fraction $Z = (1 - Z_f)y_F + Z_F(1 - y_O)$, and τ. Here $Z_f = (1+\phi)^{-1}$ is the value of Z along the stoichiometric contour. The minimum value of Z is zero at the oxidizer surface, where $y_O = 1$ and $y_F = 0$ and its maximum value is unity at the fuel surface, where $y_O = 0$, $y_F = 1$. For our problem, the maximum possible value of H is zero and the minimum possible value is -1. Functions Z and H satisfy the homogeneous forms of Eqs. (7a) and (7b), which amounts to a balance between convection and diffusion. The system of Eqs. (7a)–(7c) become

$$Pe\frac{\partial \tau}{\partial \eta} = \nabla^2 \tau + (1+\varphi)Daw \tag{9a}$$

$$Pe\frac{\partial Z}{\partial \eta} = \nabla^2 Z \tag{9b}$$

Note that the solution for H is $H = 0$ everywhere; the total enthalpy in the gas is constant. The boundary conditions for Eqs. (9a) and (9b) are

$$\tau = 0, \quad Z = 1 \text{ at } (\xi = -1, \eta \geq 0), (-1 < \xi < 0, \eta = 0) \tag{10a}$$

$$\tau = 0, \quad Z = 0 \quad \text{at } (\xi = 1, \eta \geq 0), (0 < \xi < 1, \eta = 0) \tag{10b}$$

$$\frac{\partial Z}{\partial \eta} = \frac{\partial \tau}{\partial \eta} = 0 \quad \text{at } \eta \to \infty \tag{10c}$$

The simplest case is $Pe = 0$, which produces a purely diffusive problem. The equation for Z is easily solved to give $Z = \pi^{-1}[\pi/2 - \tan^{-1}\{\tan(\pi\xi/2)/\tanh(\pi\eta/2)\}]$. The stoichiometric contour is the arc along which $Z = Z_f$, see Fig. 1(a). The trailing diffusion flame lies very near this arc, as shown.

These solutions for H and Z can be utilized to produce estimates for the heat flux to the bounding surfaces. This becomes especially straightforward in the case of infinite rate chemistry because the flame is attached to the divider, see Fig. 1(a). On the fuel side, $\nabla Z = (1 - Z_F)\nabla y_F$, whereas on the oxidizer side $\nabla Z = -Z_F \nabla y_O$. From the constancy of H, we have either $\nabla y_F = -\nabla\tau$ or $\nabla y_O = -\nabla\tau$ giving $\nabla\tau = -(1 - Z_F)^{-1}\nabla Z$ on the fuel side and $\nabla\tau = Z_F^{-1}\nabla Z$ on the oxidizer side. From the preceding solution for Z, we find

$$\nabla Z = \xi\left[\frac{-\sinh(\pi\eta/2)\cosh(\pi\eta/2)}{2\left(\sin^2\pi\xi/2 + \sinh^2\pi\eta/2\right)}\right] + \eta\left[\frac{\sin(\pi\xi/2)\cos(\pi\xi/2)}{2\left(\sin^2\pi\xi/2\sinh^2\pi\eta/2\right)}\right] \tag{11}$$

Along the lower surface $-1 < \xi < 1$, $\eta = 0$ we find

$$\nabla\tau = \frac{-\eta}{2(1 - Z_F)\tan\pi\xi/2}, \quad -1 < \xi < 0 \tag{12a}$$

$$\nabla\tau = \frac{\eta}{2Z_F\tan\pi\xi/2}, \quad 0 < \xi < 1 \tag{12b}$$

Along the vertical walls at $\xi = -1$ and $\xi = +1$, we find

$$\nabla\tau = \frac{\xi}{2(1 - Z_F)\tan\pi\eta/2}, \quad \xi = -1 \tag{13a}$$

$$\nabla\tau = \frac{-\xi}{2Z_F\tan\pi\eta/2}, \quad \xi = +1 \tag{13b}$$

From Eq. (12a), the heat flux to the divider is infinite because the flame is attached to the divider. However, the fluxes to the nearby surface may possibly be accurately represented by these equations. Part of our goal in this article is to ascertain the accuracy of Eqs. (12a) and (13a) away from the divider, and thus to determine the practical usefulness of infinite-rate Burke–Schumann heat flux calculations.

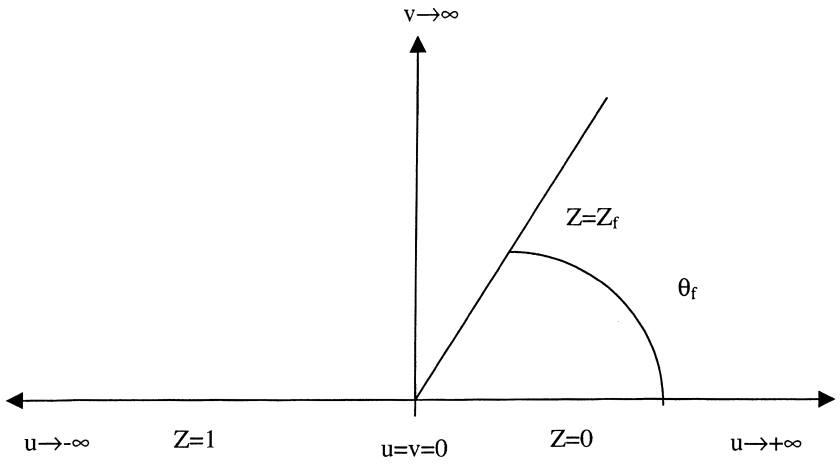

Fig. 2. Model configuration of mixture fraction Z after conformal mapping. Note that the straight diffusion flame along $Z = Z_f$ occurs only in the case of zero convection. In addition, lines of constant Z are radially-directed arcs, $Z = \theta/\pi$.

Eqs. (9a), (9b) and (10a)–(10c) will serve as a benchmark for comparing the Burke–Schumann results and the heat-transfer model results of Sections 3 and 4. These equations will be solved numerically using an Alternating Direction Implicit (ADI) method. Because the use of the mixture fraction and excess enthalpy functions de-couples the species equations from the energy equation, Eq. (9b) is solved first. Then, using the definitions of Z and H, Eq. (9a) is solved. The non-linear reaction term in Eq. (9a) is handled by using the results of the previous iteration, thus linearizing the numerical system.

3. Simplified heat transfer model 'B'

In model 'B', the flame arc becomes a constant temperature line, $\tau = 1$, extending downstream from the point r_q, see Fig. 1(b). The boundary conditions on the surfaces are $\tau = 0$ and at $\eta \to \infty$; we have the zero gradient condition $\partial\tau/\partial\eta = 0$ as before. The governing equation is $\nabla^2\tau = 0$ in the case of zero convection; $\nabla^2\tau = Pe(\partial\tau/\partial\eta)$ in the case with uniform and identical convection from the fuel and oxidizer reservoirs adjacent to the divider. The introduction of scaled coordinates $\Xi = \xi/r_q$ and $N = \eta/r_q$ places the flame leading edge at the intersection of the circular arc $R = \sqrt{\Xi^2 + N^2} = 1$ and the line $Z = Z_f$. Here, r_q is the quenching distance defined as the distance from the divider plate to the point of maximum reactivity. The flame usually quenches a very small distance upstream of the point of maximum reactivity, hence, there is no inconsistency in defining quenching distance in this manner. In the general case, this transformation offers no advantages for solution because the scaling merely changes the separation distance between the two vertical walls from 2 to $2/r_q$. When r_q becomes small, however, the vertical walls effectively disappear, and the flame sheet lies along the radially-directed arc $\theta = \pi Z_f$, $1 < R < \infty$. There are no length scales remaining in this problem, leaving a universal heat flux distribution to the lower surface given by $\partial\tau(\Xi, 0)/\partial N = g(\Xi; Z_f)$. Here, Z_f is the sole remaining parameter in the analysis. In terms of the original coordinates, we have

$$\frac{\partial\tau(\xi, 0)}{\partial\eta} = \frac{1}{r_q} g\left(\frac{\xi}{r_q}; Z_f\right) \tag{14}$$

The maximum flux occurs at the point where the derivative of $\partial\tau(\xi, 0)/\partial\eta$ vanishes.

The above expression in Eq. (14) is universal to the extent that the flame curvature can be neglected. If r_q is not sufficiently small, the curvature of the flame towards the vertical axis (see Fig. 1(a)) becomes important and the equation loses accuracy, producing an over-estimate for the surface heat flux. From Eq. (14), the integrated flux along the surface is a function only of Z_f, i.e., $\int_{-\infty}^{\infty}(\partial\tau/\partial\eta)\,d\xi = \int_{-\infty}^{\infty} g(\Xi; Z_f)\,d\Xi \equiv Q(Z_f)$. The function $Q(Z_f)$ is not symmetric about $Z_f = 1/2$ because the quench radius is asymmetric with respect to Z_f. It has been shown in Ref. [2] that Q increases as Z_f decreases, largely because of the increase in the flame temperature. This feature, we observe, is not built into this simplified model.

As shown in previous works [2,9,10], the model configuration of Fig. 1(a) can be mapped via conformal mapping methods into the configuration shown in Fig. 2. In this latter configuration, the flame is in fact a

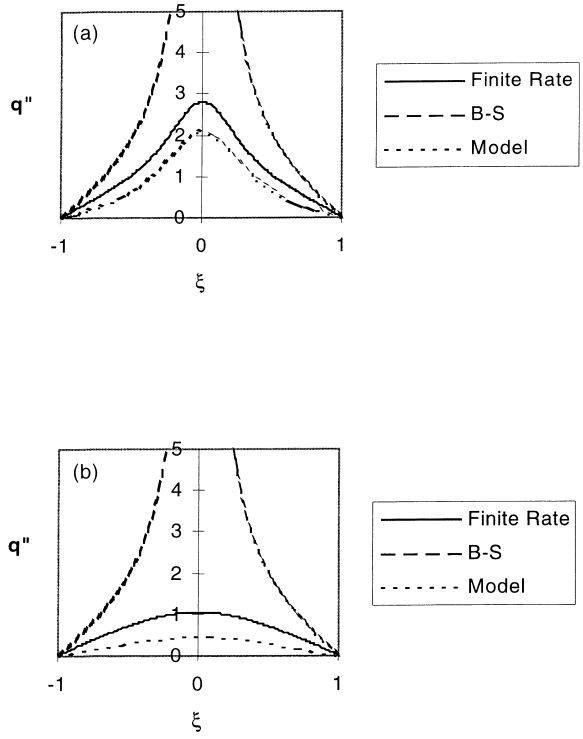

Fig. 3. (a) Heat flux profiles comparison for straight flames $r_q = 0.27$. Note the inaccuracy, generally, of the Burke–Schumann calculation of Eqs. (12a) and (12b) and the comparative similarity of the finite-rate and heat transfer model results. A scaling factor renders the latter two visually indistinguishable. Heat flux comparisons for straight flame $r_q = 0.9$. (b) Heat flux profiles comparisons for straight flames $r_q = 0.9$. The comments to (a) apply here as well.

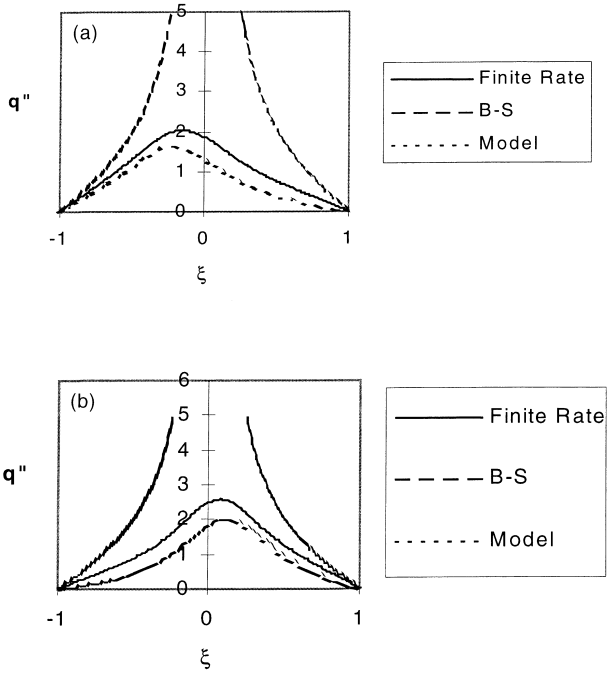

Fig. 4. (a) Heat flux profile comparisons for fuel rich flames $\phi = 0.5$, $r_q = 0.38$. For this non-symmetric case, the flux distribution is asymmetric. The Burke–Schumann model is once again a poor approximation to the heat flux. (b) Heat flux profile comparisons for fuel-lean flames $\phi = 1.5$, $r_q = 0.28$. See comments in (a).

radial arc.[1] The heat flux to the surface is $\partial\tau/\partial\eta = (\partial\tau/\partial v)(\partial v/\partial\eta)$. Analogous to the previous derivation, we define the scaled coordinates $U = u/r'_q$, $V = v/r'_q$, where $r'_q = \sqrt{u_q^2 + v_q^2}$ and $\sqrt{U^2 + V^2} = 1$ at the semi-circular arc containing the flame leading edge. Then $\partial\tau/\partial\eta = (\partial\tau/\partial V)(\partial V/\partial v)(\partial v/\partial\eta)$, with $\partial\tau(U, 0)/\partial V \equiv g(u/r'_q; Z_f)$, $\partial V/\partial v = 1/r'_q$ and $\partial v/\partial\eta = (\pi/2)\cos\pi\xi/2$ at the surface $\eta = 0$. Thus

$$\frac{\partial\tau}{\partial\eta} = g\left(\frac{\sin\pi\xi/2}{r'_q}; Z_f\right)\frac{\pi\cos\pi\xi/2}{2r'_q} \tag{15a}$$

$$r'_q = \sqrt{u_q^2 + v_q^2} = \sqrt{\sin^2(\pi\xi_q/2) + \sinh^2(\pi\eta_q/2)} \tag{15b}$$

[1] This is only strictly true in the zero convection case, $Pe = 0$.

For small ξ_q and η_q, we find $r'_q = (\pi/2)r_q$ in which case Eq. (15a) corresponds with Eq. (14).

Numerical solutions of this heat transfer model are generated in Section 4 for the heat flux to the surface.

4. Results and discussion

To begin the analysis, comparisons are made between the finite-rate chemistry model 'A', the Burke–Schumann, and the conduction heat transfer model 'B' predictions of the heat flux distribution to the lower cold boundary. Here, it is assumed that the diffusing reactants at $\eta = 0$ have the constant temperature, T_0. In Fig. 3(a) and (b), the results from each model are presented for a vertical flame with $Z_f = 1/2$ at two different quenching distances. Comparisons are also made for a fuel-lean and a fuel-rich flame in Fig. 4(a) and (b), respectively. The results presented are for the Burke–Schumann (B–S) solution for the heat flux, the heat flux obtained by solving the finite rate chemistry equations (model 'A'), and the heat flux from the simplified heat transfer model 'B'.

Examination of the stoichiometric flames in Fig. 3(a) and (b) reveal two important features. First, the B–S solution given by Eqs. (12a) and (12b) offers very different results for both large and small quench distances when compared to either the heat conduction and the finite chemistry models. Second, the simple heat conduction model captures most of the characteristics of the finite chemistry model, although the heat flux magnitude is slightly diminished. If a scaling factor is employed, better agreement is achieved. These results are for a pure diffusion flame with no convection ($Pe = 0$).

The reaction zone characteristics for model 'A' differ from those used in model 'B'. The conduction model is based on a flame sheet consisting of an infinitesimally thin reaction zone, which extinguishes a finite distance r_q from the divider plate. By contrast, the finite-rate chemistry case produces a more broadly spread reaction zone. Given this condition, it is expected that the heat transfer model will under-predict the heat loss for the pure diffusion case, as well as have a narrower peak. These characteristics are indeed observed in Figs. 3 and 4. Consistent with this, the conduction model produces better agreement with the finite rate case as the quenching distance, r_q, decreases.

For the non-symmetric case $Z_f \neq 1/2$ (see Fig. 1(a)), the flame shape will be defined by the following relation between the flame-shape coordinates ξ and η:

$$\xi = \frac{2}{\pi}\tan^{-1}\left\{\frac{\tanh\left(\frac{\pi\eta}{2}\right)}{\tan\left(\frac{\pi}{2}-\pi Z_f\right)}\right\} \tag{16}$$

Fig. 4(a) and (b) show the results for two non-stoichiometric cases. The simplified model follows well the trends of the finite rate case. The model produces a maximum heat flux at a slightly different location along the lower surface than predicted by the finite rate chemistry case. The conduction model shifts the maximum away from the divider. This can be attributed to the wider flame tip for the finite-rate chemistry case. Even with this shift the heat transfer model is closer to the finite rate chemistry case than the B–S solution. There also exists a strong asymmetry for the non-stoichiometric flames. Departures towards the fuel rich side produce closer quench distances, and consequently, larger heat losses to the lower boundary. The maximum heat flux location is also closer to the divider.

Some generalizations about the shape of the heat flux profile can be made. We wish to provide a better approximation for the heat loss profiles than those given by the readily available B–S solution. We also seek to ascertain where, if at all, the B–S solution accurately represents the heat flux to the lower boundary.

Table 1
Correction factor coefficients

ϕ	β_4	β_5	β_6	β_7	β_8
0.333	1.045	−0.179	−0.313	1.074	0.977
0.429	0.746	−0.08	−0.210	1.039	1.018
0.538	0.563	−0.096	−0.127	1.093	1.004
0.667	0.392	−0.194	−0.046	1.170	0.974
0.818	0.204	−0.084	−0.024	1.227	0.964
1.222	−0.204	0.084	−0.024	1.227	0.964
1.5	−0.392	0.194	−0.046	1.170	0.974
1.857	−0.563	0.096	−0.127	1.093	1.004
2.333	−0.746	0.08	−0.210	1.039	1.018
3.0	−1.045	0.179	−0.313	1.074	0.977

The heat flux profiles for small quenching distances ($r_q < 0.15$) obtained from model 'B' were found to collapse to a single curve. This collapse of the heat flux profiles is predicted theoretically in Section 3 by Eq. (14). The correlations were obtained for both straight flames and non-stoichiometric flames. These curve fits were obtained by using an ordinary least squares method. The correlations are non-linear so a Gauss iteration scheme was used.

For symmetric ($Z_f = 1/2$) flames, the heat flux profile can be described by the three parameter relation given below

$$q = \frac{0.572}{r_q}\mathrm{e}^{-\left|\frac{\xi}{r_q}\right|^{\beta_1}}\left(\left|\frac{\xi}{r_q}\right| + \beta_2\right)^{\beta_3} \tag{17}$$

Parameters β_1, β_2, and β_3 are 1.07, 1.01, and 0.8, respectively. Note that this result does not include any scaling factor; it is solely the shape of the heat flux profile obtained from the conduction model. Although this result is applicable only for small quenching distances, the same shape can be applied to larger quenching distances by changing the numerical parameters β_1, β_2, and β_3.

It is more challenging to model the non-symmetric flames because several quantities must be taken into account. The maximum heat loss is shifted away from the divider, and the spatial decay rates are different on each side of the maximum. The inflection points of the heat flux profile are located at several different distances from the maximum. To account for these characteristics a five parameter correction factor, $c(\xi)$, is introduced, viz.,

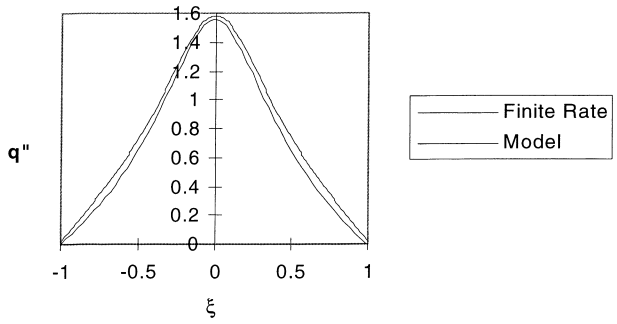

Fig. 5. Heat flux profile comparison for straight flame with convection $Pe = 1$, $r_q = 0.395$.

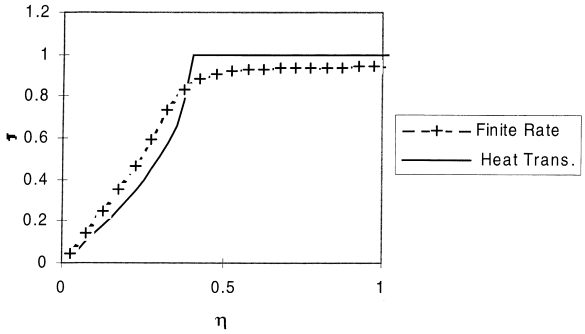

Fig. 6. Centerline temperature distributions for a straight flame $r_q = 0.375$. The broadness of the actual flame moderates the temperature variation, compared with the sharp heat transfer profile. The τ values along the diffusion flame ($\eta > 0.5$) agree to within $O(\beta^{-1})$.

$$c(\xi) = \left[\beta_4\left(\frac{\xi}{r_q} - \beta_5\right) + \beta_6\left(\frac{\xi}{r_q} - \beta_5\right)^2\right] \exp\left(-\beta_7\left|\frac{\xi}{r_q} - \beta_5\right|^{\beta_8}\right) \tag{18}$$

With this correction factor the heat flux profiles take the form

$$q = \frac{0.572}{r_q}\left(e^{-\left|\frac{\xi}{r_q}\right|^{1.07}}\left(\left|\frac{\xi}{r_q}\right| + 1.01\right)^{0.8} - c(\xi)\right) \tag{19}$$

The five parameter values are dependent on the stoichiometry parameter ϕ. Table 1 shows values of β_4 to β_8 for selected ϕ values.

The above results can be used in conjunction with a scaling factor (see Section 4.1) to obtain a good approximation for the heat flux profile to the lower boundary.

The case with convection is not considered in the numerical model or in the analytical model. However, as the discussion of Section 3 makes clear, when the quenching distance is small the heat flux profiles should closely resemble the zero-convection case. This occurs because a rescaling of the independent variables in the governing equations with r_q will eliminate the convective terms as $r_q \to 0$. Fig. 5 shows the results when $Pe = 1$. The quenching distance is computed for the finite rate chemistry case and used to determine the heat flux profile from the simple conduction model.

From Fig. 5 we observe first that the model predicts well the heat flux profile. The qualitative shape of the heat flux profile is identical to the zero convection case. Once again, it appears all that is needed for complete agreement whenever Pe is changed is the introduction of a different numerical scaling factor in Eq. (19).

4.1. Scaling factor

In order to account for the difference in reaction zone thickness between the model and the finite rate chemistry case a scaling factor S was introduced. Factor S scales the maximum heat flux from the heat transfer model to the value obtained in the finite rate chemistry case. Values of S were obtained for stoichiometric flames and then tested with non-stoichiometric flames to determine whether these values were still valid. Factor S was obtained as functions of the quenching distance, not the chemical parameters such as the Zel'dovich number, for which the dependence is much weaker than quenching distance. It is noted that the quenching distance depends on the chemical parameters. Hence, the scaling factor was correlated with the quenching distance. The relatively weaker β and Damkohler number dependence manifests itself implicitly through the effects of the reaction zone thickness on the quenching distance.

It was found that for the stoichiometric flame, S had a nearly linear dependence on r_q. The relationship is shown below

$$S = 1.72 r_q + 0.66 \tag{20}$$

Eq. (20) can be used as a direct multiplication factor in Eq. (19) for small deviations from stoichiometric flames, $0.33 < \phi < 3.0$, with S values within 10% of the numerical results.

4.2. Comparison of centerline heat losses

Examination of the temperature profile along the stoichiometric contour $Z_F = 1/2$ for vertical flames is used to verify the scaling factor, as well as to identify any shortcomings of the proposed heat transfer model.

The preliminary comparison was done for a moderately small quenching distance, $r_q = 0.375$, and a pure diffusion flame. The quenching distance was calculated by using the finite-rate chemistry code to solve for the quenching location, as defined by the maximum reactivity, as well as the vertical temperature distribution at the centerline. The resulting quench distance was employed in the heat conduction model and the temperature profile was calculated. A graphical comparison is shown in Fig. 6.

From Fig. 6 we observe that the heat conduction model underpredicts the heat loss to the divider plate. This is expected in view of the relative magnitude of the heat loss profiles to the lower boundary. Furthermore, as expected, if a ratio of the finite rate gradient to the heat transfer model gradient is examined it will produce the scaling factor S already examined. With this information, and noting that the scaling factor had a small dependence on the Zel'dovich and Damkohler numbers which will be ignored here, the gradient ratio should behave very similarly to the scaling factor with respect to r_q. We recall that S varied nearly linearly with the quenching distance. Examination of that relationship in Eq. (20) suggests that the heat conduction model gradient will approach the finite rate model gradient as the quenching distance becomes small.

Another feature shown in Fig. 6 is the different flame temperatures of the two codes. The heat conduction model assumes a flame temperature of 1.0 for the flame and uses that elevated value as its quasi-heat source. The finite rate model temperature is calculated from the set of partial differential equations shown in Section 2. The finite rate model produces a lower flame temperature, as expected, since $\tau \approx 1 - O(\beta^{-1})$. This contributes to the more gradual decline in temperature towards the lower wall, and consequentially the more linear gradient. This linear gradient supports the simplified notion of assuming a linear profile from the quench location to the wall [2,10]. However, this assumption is typically based on an adiabatic flame temperature close to unity (i.e., $\beta \to \infty$ limit), and does not take into account any heat losses through the reaction zone. The heat loss from the reaction zone in the finite-rate model 'A' is evident beginning near $\eta = 0.5$ and continuing to the location of the heat-transfer model flame tip at $\eta = 0.375$.

4.3. Comparison to finite-chemistry model [2,9]

A comparison of our heat transfer results may be made to the finite-rate chemistry model examined in Refs. [2,10]. The heat transfer cold wall beneath the flame leading edge is given by

$$q = \frac{\vartheta}{b_q^{3/2}} \sqrt{\frac{Da}{\beta^3}} \frac{4}{\pi} (1 - Z_f)^{1/2} \sin^2(\pi Z_f) \tag{21}$$

where

$$\vartheta = 1 + \left\{ (1 - Z_f) \left(\frac{\sin \pi(Z_f - \delta_O)}{\sin \pi Z_f} - 1 \right) + Z_f \left(\frac{\sin \pi(Z_f + \delta_F)}{\sin \pi Z_f} - 1 \right) \right\} \tag{22a}$$

$$b_q = 3.752 \left\{ 1 - \exp\left(-7.366 Z_f^{1.71} \right) \right\} Z_f^{0.36} \tag{22b}$$

and $\delta_O = Z_f(1 - \tau_q)$, $\delta_F = (1 - Z_f)(1 - \tau_q)$, where τ_q, the flame leading edge quenching temperature, is given by $1 - \kappa/\beta$. It is shown in Section 4.2 of Ref. [2] that a value of κ between 1.5 and 2 is reasonable. We use $\kappa = 1.75$. For the symmetric case $Z_f = 1/2$, we find $\delta_O = \delta_F = \kappa/2\beta$, whereby $\vartheta = \cos(\pi\kappa/2\beta)$ and $b_q = 2.62$, giving $q = 0.21 \cos(\pi\kappa/2\beta)(Da/\beta^3)^{1/2}$.

The use of $\kappa = 1.75$, and $\beta = 8.0$ gives the estimate $q \cong 0.198(Da/\beta^3)^{1/2}$. In order to relate this result to the quench distance, we employ Eq. 8 of Ref. [2], which gives

$$r_q = \frac{2}{\pi} \frac{b_q^{3/2}}{4 Z_f (1 - Z_f)^{3/2}} \sqrt{\frac{\beta^3}{Da}} \tag{23}$$

where we have used the factor $\pi/2$ to convert r_q' of Eq. 8 of Ref. [2] from the u–v system of coordinates to the $\xi - \eta$ coordinates used here, as outlined in Section 3, see Eq. (15b) et seq. The preceding numbers give $r_q \cong 3.82(\beta^3/Da)^{1/2}$, whereby, $q \cong 0.76/r_q$, which compares favorably with Eq. (17), $q \cong 0.57/r_q$, especially when we consider that the latter must be multiplied by a scaling factor greater than unity given by Eq. (20).

Consequently, the heat transfer model prediction is functionally consistent with the more detailed finite chemistry model. In addition, and in contrast with Ref. [2], the heat transfer model produces an expression for the distribution of q along the entire surface, not only its maximum value. For this reason, it is possible to replace the factor $0.572/r_q$ in Eq. (17) with Eq. (21), using Eqs. (22a) and (22b) for ϑ and b_q, respectively. The pure heat transfer formula now includes the influences of finite-rate one-step chemistry. A similar replacement, of course, may be made in Eq. (19) for the asymmetric case.

4.4. Zel'dovich number effects

As stated previously, the temperature gradients at the lower boundary produced by the two models show better agreement as r_q decreases. That is not to say

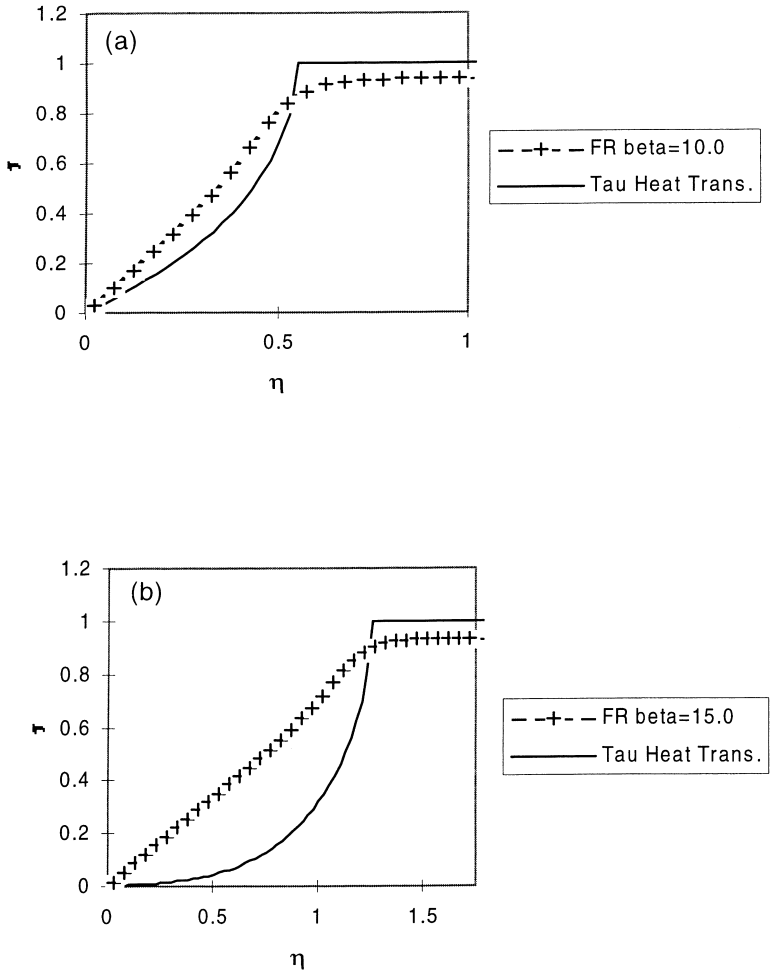

Fig. 7. (a) Centerline temperature profile for a straight flame $r_q = 0.525$. (b) Centerline temperature distribution for a straight flame $r_q = 1.225$. For large quench distances the pure heat transfer temperature profile differs significantly from the finite-rate chemistry profile.

that the profiles become more similar under this criterion. The presented profiles can be divided into three general regions: the flame tip region, the wall region, and the transition region which connects the two aforementioned regions. As will become evident from Fig. 7(a) and (b) below, the transition region between the two models have distinctly different shapes. The conduction model produces a much steeper gradient immediately after the flame tip and a much smaller gradient at the wall. Hence, the transition region is much more curved than the nearly linear temperature profile produced by finite rate chemistry model. Having noted that the profiles agree well in the wall region when the flame quenches very close to the lower boundary and that the transition regions will have their own characteristics, it is of interest to find the conditions where the flame tip regions exhibit agreement.

The finite rate model produces a flame temperature that is lower than the adiabatic flame temperature. This suggests that for the flame tip regions to agree, the finite rate model should produce a flame temperature closer to the adiabatic temperature assumed for the conduction model. This can be achieved by increasing the Zel'dovich number, β, which also has the effect of increasing the quench distance. This produces a higher flame temperature and lower heat losses through the flame tip, thus improving agreement in the flame tip region of the temperature profiles. However, the gain in agreement in one region reduces it in another, as can be seen in Fig. 7(a) and (b). Agreement may also require an unrealistically large value of β.

The Zel'dovich number also depends on the wall temperature T_0 through the relation $\beta = (E/RT^2) \times (T_f - T_0)$. When all quantities other than T_0 are fixed,

it is possible to examine the influences of wall temperature on heat flux and flame quenching distance. Since $q \approx 0.57/r_q$ and $r_q \propto (T_f - T_0)^{3/2}$, we find $q \propto (T_f - T_0)^{-3/2}$, $dr_q/dT_0 \propto -(T_f - T_0)^{1/2}$, $dq/dT_0 \propto (T_f - T_0)^{-5/2}$. Thus, as T_0 increases r_q vanishes at a successively decreasing rate, while q increases at a successively increasing rate. Under practical conditions, we expect that the near-wall flame tip can heat the wall, raising T_0 and decreasing r_q, while increasing q. It is not clear how long this incremental process can continue, for there are upper bounds on the chemical production of heat that leads to q.

4.5. Characteristic flame-tip width

For small r_q, a practical estimate of the width of the triple-flame structure, shown as the lowermost arc of Fig. 1(a), is obtained by exploiting the relationship for $q(\xi)$ given by Eq. (17). We note the closeness of β_1, β_2, and β_3 to unity and write $q(\xi) \approx C \exp(-\xi/r_q)(1 + \xi/r_q)$, where $C = 0.572/r_q$. This function possesses an inflection point at $\xi = r_q$, which we interpret as a measure of the triple-flame tip structure half-width, l_r. Thus, we write

$$l_r \approx 2r_q \propto \beta^{3/2} \exp(E/2RT_f) \tag{24}$$

This result agrees with a previously derived estimate [13]. As the flame temperature increases, all remaining constant, both β and the exponential factor decrease. Hence, l_r decreases exponentially and algebraically as flame temperature increases. Conversely, as the non-dimensional activation energy increases, l_r increases exponentially.

4.6. The q–r_q relationship

In our study, the relation (17) was derived for infinite-rate chemistry, and the modifications of Section 4.3 were appended under the approximation that the infinite-rate chemistry limit was a reasonably accurate approximation. In this case, the essential prediction is $qr_q \sim O(1)$ and constant. We expect this relation to apply in a broad middle range, but not at the extremes $q \to \infty$ ($r_q \to 0$) and $q \to 0$ ($r_q \to \infty$). The latter limit may be interpreted as flame liftoff, whereas the former as flame extinction. Liftoff, followed eventually by blowoff, occurs when heat losses to solid boundaries cannot be sustained. The separation distance between surface and flame increases until the flame effectively no longer interacts with the surface. At blowoff, even gas-phase flaming becomes impossible. Extinction, on the other hand, occurs when the flame loses too much heat to the surface to survive. It produces enough heat that lifting is not necessary, but the losses to the surface become excessive. Or numerical integrations have in fact produced both limiting cases, although the detailed description is beyond the scope of this article. Nevertheless, it appears that the extinction limit is attainable without radiant losses from the flame tip, without thermal expansion of the gas, or without buoyancy. All that is required for a minimalist description is chemical heat production and conductive surface losses.

5. Conclusions

The conductive heat transfer sub-model reproduces many of the global features of the finite rate chemistry case. The profiles at the lower boundary are similar for both models with only a scaling factor needed to produce accurate agreement. However, when examining the temperature profiles along the centerline of the lifted flame the two models can produce significantly different results for the transition region and the flame tip region, especially as the quenching distance increases. This can be partially attributed to the assumption of a flame sheet in the heat transfer model, which differs from the non-zero flame thickness produced by finite rate chemistry. The conduction heat transfer model is unable to accurately predict the heat loss from the flame tip, even for pure diffusion flames. For this reason the conduction model is not useful for describing thermal phenomena close to the flame tip, but is very useful in examining events away from this region as is generally true for other heat transfer models of detailed flame process [5]. This limitation might be overcome by introducing a volumetric heat generation term into the conduction model that has temperature dependence, but this is a subject for future study.

For modeling finite rate chemistry influences on the heat flux, we recommend a combination of Eqs. (17) [or (19) and (21)], with the later being substituted for the factor $0.572/r_q$ appearing in the formula. This combined equation accurately predicts the flux beneath the flame leading edge and also its distribution along the surface.

It is also noted that the results obtained herein may be limited to configurations closely resembling the slot configuration used in this work. The heat flux profiles for other lifted flames with different physical and flow orientations may produce different correlations. It is a limitation of the work that the methods used here will need to be followed for different problems. However, the usefulness of the results is not diminished for this lack of adaptability. The general result of our research is to show that beneath the flame tip $q \sim O(1/r_q)$, where $r_q \sim O([\beta^3/Da]^{1/2})$, to within a multiplicative function of global stoichiometry. Although this result may be deduced by simple dimensional analysis and

scaling arguments, we have in addition quantified the heat flux distribution beneath the flame tip.

Acknowledgements

Support provided for this research by NASA Microgravity Combustion program contract no. NAC3-1626, is gratefully acknowledged. Dr. Vedha Nayagem served as contract monitor.

References

[1] F. Nietzsche, Towards a psychology of the artist, Twilight of the Idols (R.J. Hollingdale, Trans.), Penguin, London, 1968.
[2] I.S. Wichman, Z. Pavlova, B. Ramadan, G. Qin, Heat flux from a diffusion flame tip to an adjacent surface, Combustion and Flame 1998, in press.
[3] I.S. Wichman, B. Ramadan, Theory of attached and lifted diffusion flames, Phys. of Fluids 10 (12) (1998).
[4] F.A. Williams, Combustion Theory, 2nd ed, Benjamin/Cummings, Menlo Park, CA, 1985.
[5] I.S. Wichman, F.A. Williams, A simplified model of flame spread in an opposed flow along a flat surface of a semi-infinite solid, Combustion Science and Technology 32 (1983) 91–123.
[6] C. DiBlasi, I.S. Wichman, Effects of solid-phase properties on flames spreading over composite materials, Combustion and Flame 102 (1995) 229–240.
[7] I.S. Wichman, N. Lakkaraju, B. Ramadan, The structure of quenched triple flames near cold walls in convective flows, Combustion Science and Technology 127 (1997) 141–165.
[8] B. Ramadan, Personal communications, 1997–1998.
[9] I.S. Wichman, On the quenching of a diffusion flame near a cold wall, Combustion Science and Technology 64 (1989) 295–313.
[10] I.S. Wichman, Z. Pavlova, B. Ramadan, Attachment of diffusion flames near cold, chemically inert surfaces with and without reactant flow, MSU CRL 09-24-96 (1996).
[11] M.L. Rightly, F.A. Williams, Analytical approximations for structures of wet CO flames with one-step chemistry, Combustion and Flame 101 (3) (1995) 287–301.
[12] P. Hsu, R.D. Matthews, Necessity of using detailed kinetics in models for premixed combustion within porous media, Combustion and Flame 93 (4) (1993) 457–466.
[13] I.S. Wichman, B. Ramadan, Theory of attached and lifted diffusion flames, Physics of Fluids A 10 (12) (1998) 3145–3154.